Am J Cancer Res 2022;12(5):2032-2049
www.ajcr.us /ISSN:2156-6976/ajcr0141481

Original Article

A novel preoperative MRI-based radiomics nomogram outperforms traditional models for prognostic prediction in pancreatic ductal adenocarcinoma

Hui Qiu[1,2*], Muchen Xu[3*], Yan Wang[2], Xin Wen[1,2], Xueting Chen[2], Wanming Liu[2], Nie Zhang[2], Xin Ding[1,2], Longzhen Zhang[1,2]

[1]Cancer Institute, Xuzhou Medical University, Xuzhou 221000, Jiangsu, China; [2]Department of Radiation Oncology, Affiliated Hospital of Xuzhou Medical University, Xuzhou 221000, Jiangsu, China; [3]Department of Radiation Oncology, Dushu Lake Hospital Affilated to Soochow University, Medical Center of Soochow University, Suzhou 215000, Jiangsu, China. [*]Equal contributors.

Received January 2, 2022; Accepted April 15, 2022; Epub May 15, 2022; Published May 30, 2022

Abstract: To develop an efficient prognostic model based on preoperative magnetic resonance imaging (MRI) radiomics for patients with pancreatic ductal adenocarcinoma (PDAC), the preoperative MRI data of PDAC patients in two independent centers (defined as development cohort and validation cohort, respectively) were collected retrospectively, and the radiomics features of tumors were then extracted. Based on the optimal radiomics features which were significantly related to overall survival (OS) and progression-free survival (PFS), the score of radiomics signature (Rad-score) was calculated, and its predictive efficiency was evaluated according to the area under receiver operator characteristic curve (AUC). Subsequently, the clinical-radiomics nomogram which incorporated the Rad-score and clinical parameters was developed, and its discrimination, consistency and application value were tested by calibration curve, concordance index (C-index) and decision curve analysis (DCA). Moreover, the predictive value of the clinical-radiomics nomogram was compared with traditional prognostic models. A total of 196 eligible PDAC patients were enrolled in this study. The AUC value of Rad-score for OS and PFS in development cohort was 0.724 and 0.781, respectively, and the value of Rad-score was negatively correlated with PDAC's prognosis. Moreover, the developed clinical-radiomics nomogram showed great consistency with the C-index for OS and PFS in development cohort was 0.814 and 0.767, respectively. In addition, the DCA demonstrated that the developed nomogram displayed better clinical predictive usefulness than traditional prognostic models. We concluded that the preoperative MRI-based radiomics signature was significantly related to the poor prognosis of PDAC patients, and the developed clinical-radiomics nomogram showed better predictive ability, it might be used for individualized prognostic assessment of preoperative patients with PDAC.

Keywords: Pancreatic ductal adenocarcinoma, radiomics, nomogram, prognostic model

Introduction

Pancreatic ductal adenocarcinoma (PDAC), which accounts for approximately 80% of all pancreatic tumors, is the most common primary malignant tumor of the pancreas [1]. Because of its stubborn characteristics of tending to rapid progression and resistance to chemotherapy and radiotherapy, the 5-year survival rate of PDAC usually do not exceed 5% [2, 3]. As one of the most important and potentially curable treatments, surgical resection is appropriate for only about 20% of newly diagnosed PDAC patients [4]. Even with complete resection (R0), the risk of recurrence within 5 years remains high (more than 75%) [5]. Currently, there are evidence demonstrate that neoadjuvant therapy can improve the R0 resection rate and disease-free survival of resectable PDAC patients, however, multiple clinical trials have shown that the preoperative treatment does not significantly improve patients' overall survival (OS) [6], this means that not all PDAC patients benefit from neoadjuvant therapy. Hence, accurate screening of patients with poor prognosis and giving them timely neo-

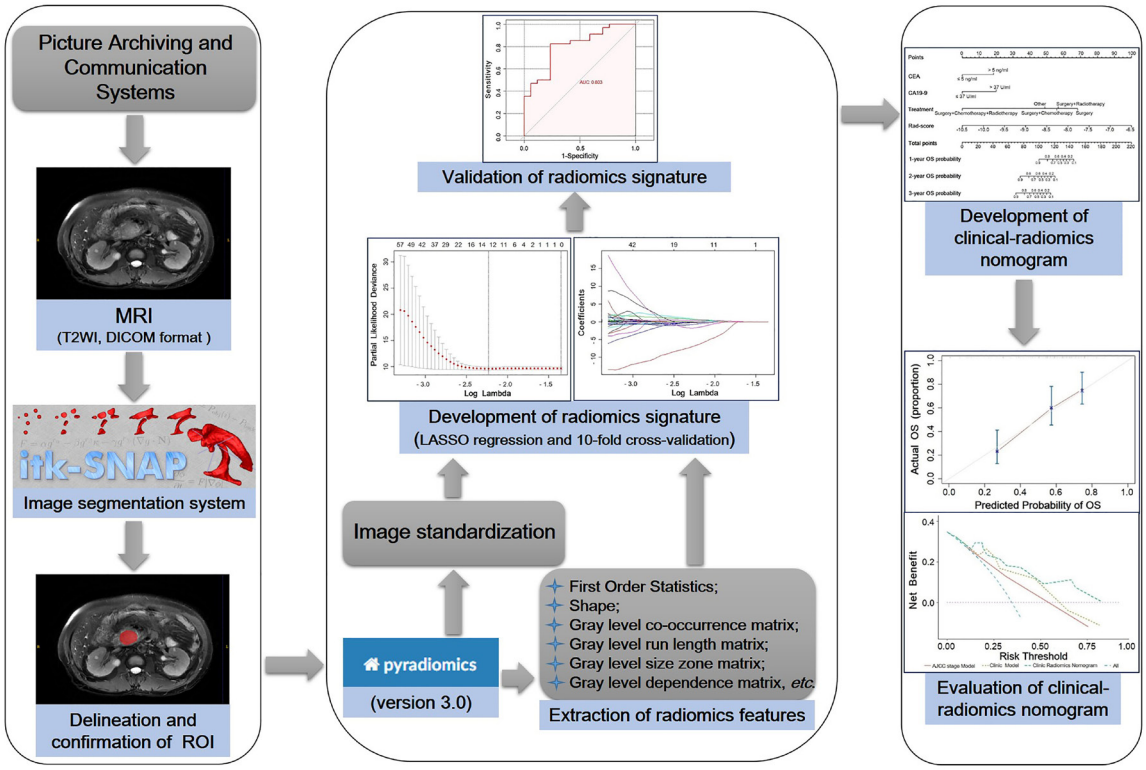

Figure 1. Workflow of the development of the clinical-radiomics nomogram.

adjuvant therapy are very important to improve the overall prognosis of patients with PDAC.

Currently, the validated clinical prognostic models for PDAC mainly include American Joint Committee on Cancer (AJCC) TNM staging system and the levels of tumor markers, nevertheless, the accuracy of AJCC staging system might vary depending on tumor location [7] and it needs to be based on postoperative pathological data, so it is not helpful for preoperative prediction of patients' prognostic risk. In addition, some studies have shown that there was no significant correlation between preoperative tumor marker levels and PDAC patients' survival [8, 9]. Therefore, an efficient prognostic model with high clinical applicability is urgently needed to predict the survival of preoperative patients with PDAC. Due to the spatial heterogeneity of solid tumors, to some extent, the precision of molecular markers based on pathological specimens in predicting patients' prognosis is reduced. However, this heterogeneity offers great potential for medical imaging, which can capture the heterogeneity within tumors in a non-invasive way [10].

From this, the concept of "radiomics" was firstly proposed by Lambin P. *et al.* in 2012 [10]. Radiomics can extract large amounts of image features from radiographic images in a high-throughput way, and use feature algorithm to deeply excavate and analyze these data, so as to provide more information reflecting internal heterogeneity and biological behavior of malignancies for clinical decision making [10, 11].

At present, the development of radiomics in tumors mainly include diagnosis, prognostic prediction, preoperative staging and assessment of treatment response [12-15]. Previous studies have shown that computed tomography (CT)-based radiomics was significantly associated with PDAC patients' prognosis [9, 16], however, radiomics based on magnetic resonance imaging (MRI), which has superior soft tissue contrast to CT, have been poorly studied in predicting the prognosis of PDAC, and most of the previous studies were focused on the evaluation of early recurrence [17], response to treatments [18] and preoperative prediction of tumor-infiltrating lymphocytes [19]. Therefore, it is of certain clinical value to

Table 1. Clinical characteristics of enrolled patients

Variables	Development cohort (*n*, %)	Validation cohort (*n*, %)	*P*
Gender			0.643
Male	77 (53.1%)	29 (56.9%)	
Female	68 (46.9%)	22 (43.1%)	
Age, years			0.872
≤ 60	53 (36.6%)	18 (35.3%)	
> 60	92 (63.4%)	33 (64.7%)	
Tumor location			0.321
head	125 (86.2%)	41 (80.4%)	
body and tail	20 (13.8%)	10 (19.6%)	
Maximum diameter of tumor			0.071
≤ 4 cm	92 (63.4%)	25 (49.0%)	
> 4 cm	53 (36.6%)	26 (51.0%)	
Differentiated degree			0.805
High	15 (10.3%)	7 (13.7%)	
Medium	92 (63.4%)	31 (60.8%)	
Low	38 (26.2%)	13 (25.5%)	
AJCC staging			0.848
I	23 (15.9%)	7 (13.7%)	
II	96 (66.2%)	36 (70.6%)	
III	26 (17.9%)	8 (15.7%)	
T staging			0.192
T1	24 (16.6%)	6 (11.8%)	
T2	68 (46.9%)	19 (37.3%)	
T3	53 (36.6%)	26 (51.0%)	
N staging			0.872
N0	49 (33.8%)	17 (33.3%)	
N1	69 (47.6%)	26 (51.0%)	
N2	27 (18.6%)	8 (15.7%)	
Vascular invasion			0.423
No	73 (50.3%)	29 (56.9%)	
Yes	72 (49.7%)	22 (43.1%)	
Nerve invasion			0.226
No	71 (49.0%)	30 (58.8%)	
Yes	74 (51.0%)	21 (41.2%)	
BMI (Kg/m^2)			0.686
< 24	72 (49.7%)	27 (52.9%)	
≥ 24	73 (50.3%)	24 (47.1%)	
CEA (ng/ml)			0.639
≤ 5	36 (24.8%)	11 (21.6%)	
> 5	109 (75.2%)	40 (78.4%)	
CA19-9 (U/ml)			0.906
≤ 37	64 (44.1%)	23 (45.1%)	
> 37	81 (55.9%)	28 (54.9%)	
Smoking history			0.201
No	110 (75.9%)	34 (66.7%)	
Yes	35 (24.1%)	17 (33.3%)	

develop a prognostic model based on MRI radiomics for PDAC.

In this study, we used related algorithm to extract and screen out the radiomics features of preoperative MRI images which were significantly relevant to the prognosis of PDAC, and calculated the score of radiomics signature (Rad-score), then a clinical-radiomics nomogram was developed and externally validated. The analysis showed that the preoperative MRI-based radiomics nomogram could effectively predict the OS and progression-free survival (PFS) in patients with PDAC, which may potentially help to make the personalized therapy in PDAC.

Materials and methods

Patients

In this two-center retrospective prognostic study, patients with pathologically diagnosed PDAC in the Affiliated Hospital of Xuzhou Medical University and Taizhou People's Hospital from January 2013 to December 2019 were selected according to the following inclusion and exclusion criteria, the cases from the Affiliated Hospital of Xuzhou Medical University were included in the development cohort, and the cases from Taizhou People's Hospital were included in the validation cohort. Inclusion criteria: (1) over 18 years old; (2) patients who did not receive preoperative anti-cancer therapies such as radiotherapy, chemotherapy, targeted therapy and/or immunotherapy; (3) preoperative MRI images were available within 2 weeks before surgery. Exclusion criteria: (1) lacking complete clinical data and follow-up data; (2) simultaneously combined with other malignant tumors; (3) patients who died of surgical complications within 30 days after surgery; (4) the quality of MRI images was poor.

Drinking history			0.33
No	107 (73.8%)	34 (66.7%)	
Yes	38 (26.2%)	17 (33.3%)	
Hypertension			0.51
No	98 (67.6%)	37 (72.5%)	
Yes	47 (32.4%)	14 (27.5%)	
Diabetes			0.269
No	116 (80.0%)	37 (72.5%)	
Yes	29 (20.0%)	14 (27.5%)	
Clinical symptoms			0.29
No	8 (5.5%)	5 (9.8%)	
Yes	137 (94.5%)	46 (90.2%)	
Therapeutic regimen			0.935
Surgery alone	61 (42.1%)	22 (43.1%)	
Surgery + chemotherapy	67 (46.2%)	23 (45.1%)	
Surgery + radiotherapy	3 (2.1%)	1 (2.0%)	
Surgery + chemoradiotherapy	2 (1.4%)	0 (0.0%)	
Other	12 (8.3%)	5 (9.8%)	

Collection of clinical data and segmentation of region of interest

The following clinical parameters of enrolled patients were collected from the electronic medical records system, including: gender, age, clinical symptoms, tumor location, the maximum diameter of tumor, differentiated degree, TNM stage (according to the 8th edition of AJCC staging system), vascular invasion, neurological invasion, body mass index (BMI), levels of carcino-embryonic antigen (CEA) and carbohydrate antigen 19-9 (CA19-9), smoking and drinking history, history of hypertension and diabetes, therapeutic regimen. The follow-up ended on December 30, 2020, and the primary endpoints were OS and PFS.

The preoperative MRI images of all enrolled patients were taken from the Picture Archiving and Communication Systems (PACS) and exported in digital imaging and communications in medicine (DICOM) format. Since the MRI scanning equipments, scanning sequences and parameters were different in the two centers, in order to minimize the bias caused by confounding factors, only T2-weighted imaging (T2WI) sequence was used for subsequent radiomics analysis in this study. MRI images in DICOM format were imported into the image segmentation system ITK-SNAP (version 3.6.0, www.itksnap.org), and the region of interest (ROI) was manually delineated along the tumor edge at the layer of maximum diameter to extract radiomics features (**Figure 1**). The final ROIs were reviewed and confirmed by multiple senior radiation oncologists who were masked to the patients' clinical outcomes, any disagreements were resolved by consensus.

Extraction of radiomics features

In order to minimize the bias caused by non-tumor-related factors, we used Pyradiomics (version 3.0) to conduct the standardized preprocessing of MRI images and the extraction of radiomics features. Using the internal parameters of "Setting" to set the following parameters: "Normalize", "normalizeScale", "interpolator", "resampledPixelSpacing", "binWidth" and "voxelArrayShift". Setting the following parameters in "Image Type": original, laplacian of gaussian filter (LoG) and wavelet filter. Based on all possible combinations of high (H)-pass filter and low (L)-pass filter, eight types of wavelet features were obtained and labeled as LLH, LHL, LHH, HLL, HLH, HHL, HHH and LLL. Setting the following parameters in "Feature": first order statistics, shape, gray-level co-occurrence matrix (GLCM), gray-level run length matrix (GLRLM), gray-level size zone matrix (GLSZM), gray-level dependence matrix (GLDM), *etc*.

In order to avoid the overfitting of feature data, the least absolute shrinkage and selection operator (LASSO) regression analysis was used to conducting dimensionality reduction of radiomics features in the development cohort. Using LASSO-Cox regression model and 10-fold cross-validation to screen out the optimal radiomics features with non-zero coefficients.

Development and evaluation of radiomics signature

We then used the optimal radiomics features to build the radiomics signature and weighted these features with their corresponding regression coefficients, and finally summed them up to obtain Rad-score for each patient. Area under the curve (AUC) was calculated using receiver operator characteristic (ROC) curve to assess the accuracy of radiomics signature in predicting prognosis. According to Rad-score's optimal truncation value which was determin-

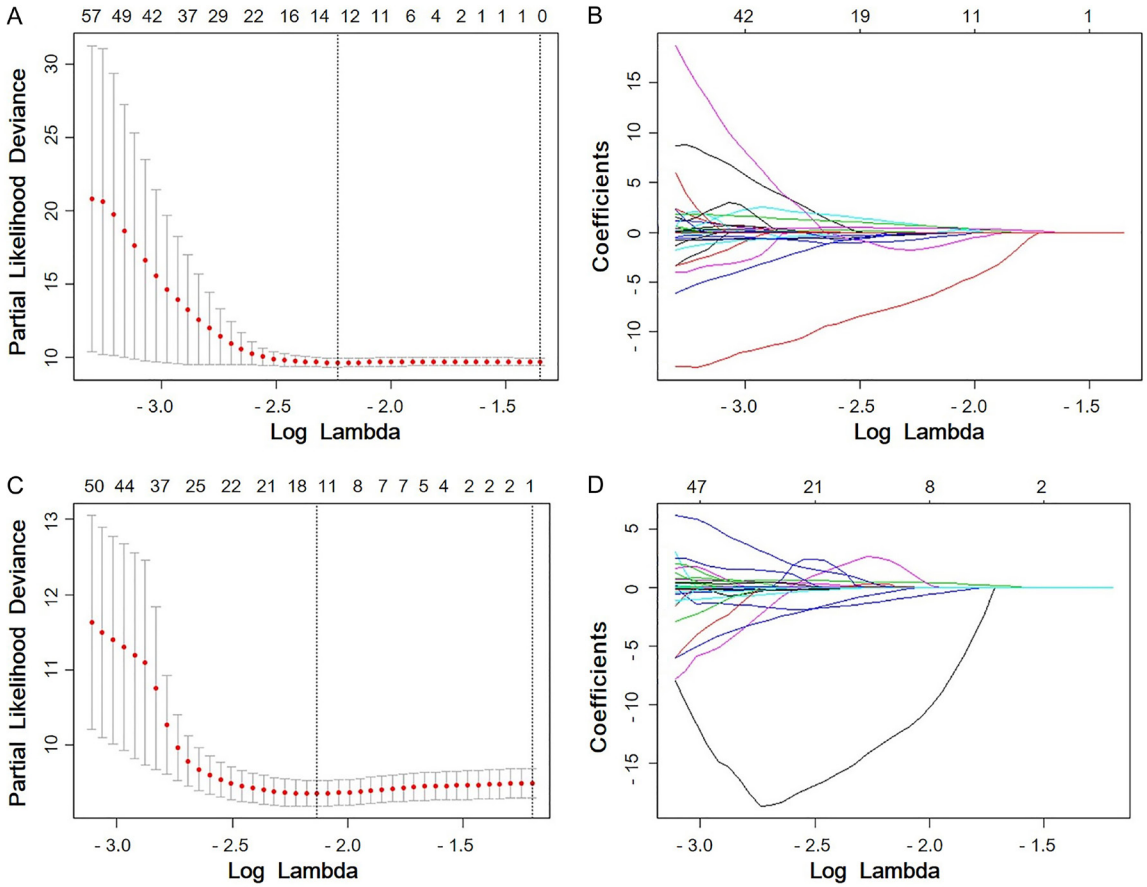

Figure 2. Selection of the optimal radiomics features from the development cohort. Tuning parameter (lambda) selection in least absolute shrinkage and selection operator regression analysis for OS (A) and PFS (C) used 10-fold cross-validation as the minimum criteria. The log lambda (x-axis) is plotted against the partial likelihood deviance (y-axis). The vertical lines are drawn at the optimal value of lambda for OS (lambda = 0.107315, B) and PFS (lambda = 0.118474, D).

ed by the Jorden index, all patients were divided into high Rad-score group and low Rad-score group, baseline characteristics and prognosis were then compared between the two groups.

Development and assessment of the clinical-radiomics nomogram

Univariate Cox regression was first used to analyze the relationship between clinical parameters, Rad-score and the prognosis of PDAC. Variables with $P < 0.05$ were then included into the multivariate analysis to determine the independent risk factors of prognosis, which were subsequently used to develop a novel clinical-radiomics nomogram to predict the OS and PFS. We then performed internal validation and external validation in the development and validation cohorts, respectively, and tested the predictive efficacy of this clinical-radiomics nomogram by calculating the concordance index (C-index). A calibration curve was plotted with 1000 resamples to assess the consistency between the observed risk and the predicted risk of the nomogram.

In addition, two additional predictive models were used to assess the prognosis, one model was based on the 8th AJCC staging system of PDAC and the other was based on independent risk factors among clinical parameters. Subsequently, decision curve analysis (DCA) was used to compare the prognostic value of clinical-radiomics nomogram with the above two models, and to analyze the clinical application value of this nomogram by quantitatively measuring the net benefit under different threshold probabilities.

Statistical analysis

In this study, SPSS software (version 25.0) and R software (version 3.6.1) were used for statis-

Table 2. Optimal radiomics features associated with prognosis and their corresponding coefficients from the development cohort

	Feature	Coefficent
OS	original_gldm_DependenceVariance	-0.203855455575152
	log.sigma.5.0.mm.3D_glcm_Imc2	0.724545023945380
	wavelet.LLH_firstorder_10Percentile	0.000594508043691
	wavelet.LLH_firstorder_Mean	0.000600990342681
	wavelet.LHL_glcm_Correlation	0.673884692402828
	wavelet.LHL_glcm_DifferenceEntropy	-0.151955758019423
	wavelet.LHL_glszm_ZoneVariance	0.425537714201555
	wavelet.LHH_glszm_SmallAreaEmphasis	-0.664303013620779
	wavelet.HLL_glcm_Imc2	-1.666710281139970
	wavelet.HLH_glcm_DifferenceVariance	-0.001120927223751
	wavelet.HLH_glcm_Imc2	-6.692539643367370
	wavelet.HHL_glcm_ClusterShade	0.000129507265119
PFS	original_glrlm_LongRunEmphasis	-0.971744337864066
	wavelet.LLH_firstorder_10Percentile	0.000714077093010
	wavelet.LLH_firstorder_Kurtosis	0.008034973600428
	wavelet.LHL_glszm_LargeAreaEmphasis	0.046151959378921
	wavelet.LHL_glszm_ZoneVariance	0.455979566294932
	wavelet.LHH_firstorder_Uniformity	1.914692649179020
	wavelet.LHH_glcm_Imc2	-12.453403725496700
	wavelet.HLH_glcm_Contrast	-0.000001700231086
	wavelet.HLH_glcm_DifferenceVariance	-0.001502869327855
	wavelet.HHL_glcm_ClusterShade	0.000118729830465
	wavelet.HHL_glszm_LargeAreaLowGrayLevelEmphasis	-0.221256029568318

tical analysis. The normality of quantitative data was tested by Kolmogorov-Smirnov method. Continuous variables are expressed as mean and standard deviation and compared by independent-sample *t* test, whereas categorical variables are expressed as the frequency and proportion and compared by Chi-square test or Fisher's exact test, when appropriate. Cox regressions analysis was used to assess the association of variables with OS and PFS and calculate the hazard ratios (HRs) and 95% confidence intervals (CIs). Differences in OS and PFS between high Rad-score group and low Rad-score group were estimated with Kaplan-Meier method and compared by Log-rank test. $P < 0.05$ was considered statistically significant.

Results

The clinical characteristics of enrolled patients

After strict screening, a total of 196 eligible PDAC patients were enrolled in this study, including 145 cases in development cohort and 51 cases in validation cohort, all patients received R0 resection, and their clinical characteristics were shown in **Table 1**, and there were no significant difference in clinical characteristics between the two groups. The median follow-up was 222 days, and no distant metastasis was observed before surgery, 61 patients (31.12%) developed local recurrence and distant metastasis during postoperative follow-up.

The radiomics signature was developed based on optimal radiomics features

In this study, 960 radiomics features were obtained from the ROI in the development cohort. After dimensionality reduction, the number of optimal radiomics features which were dramatically related to OS and PFS were 12 and 11, respectively (**Figure 2**; **Table 2**), and most of the optimal radiomics features were wavelet filter and GLCM related, among them, "wavelet.HLH_glcm_Imc2" had a significant negative correlation with OS with a coefficient

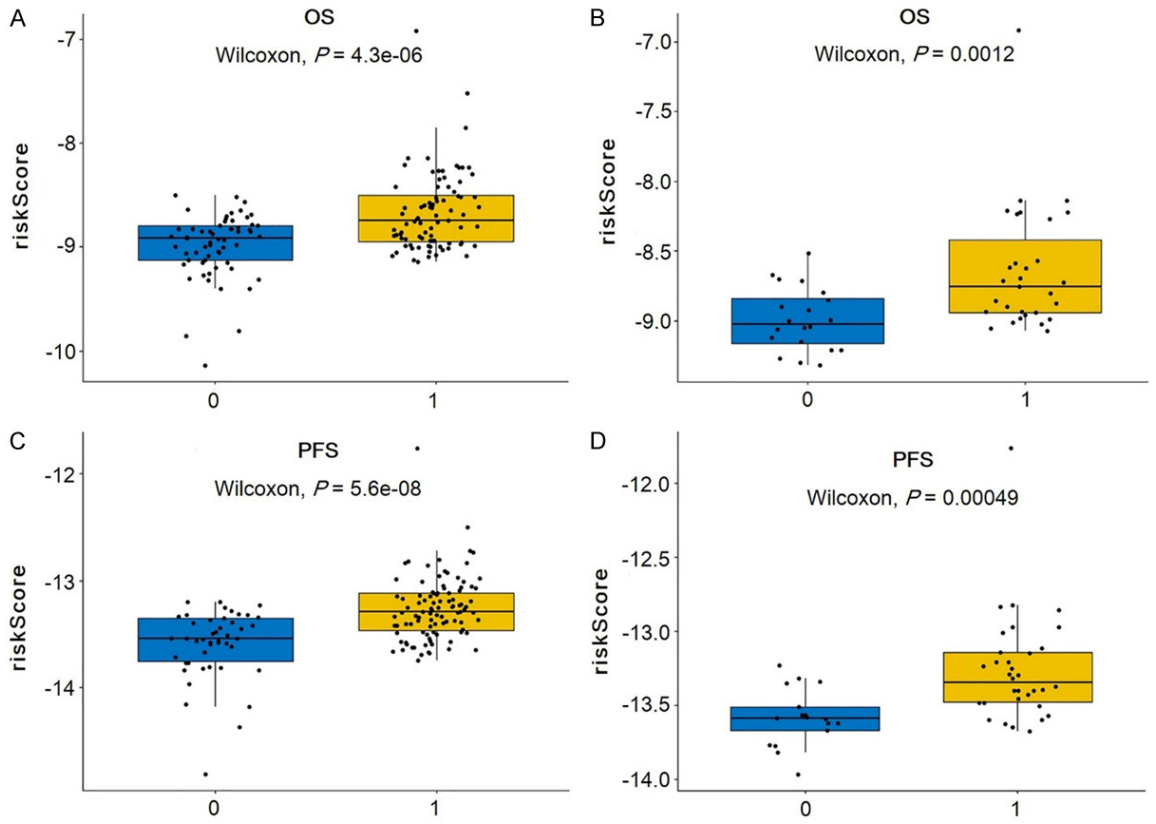

Figure 3. The value level of Rad-score among PDAC patients under different survival or disease states. The distribution of Rad-score for OS in development cohort (A) and validation cohort (B). 0 (blue) represents alive population, and 1 (yellow) represents dead population. The distribution of Rad-score for PFS in development cohort (C) and validation cohort (D). 0 (blue) represents progression-free survival, and 1 (yellow) represents recurrence, metastasis and/or death.

of -6.69, while "wavelet.LHH_glcm_Imc2" had a significant negative correlation with PFS with a coefficient of -12.45. Then we used these radiomics features to build the radiomics signature, and the OS- or PFS-related Rad-score (named Rad-score_OS or Rad-score_PFS) were calculated based on the formula as shown in Supplementary Figure 1. Subsequently, we analyzed the distribution of Rad-score_OS and Rad-score_PFS in PDAC patients with different survival states. The results showed that, in both the development and validation cohorts, the value of Rad-score_OS of dead patients was significantly higher than alive population (**Figure 3A** and **3B**), and the value of Rad-score_PFS of patients who suffered from cancer recurrence, metastasis and/or death was obviously higher than those without disease progression (**Figure 3C** and **3D**).

ROC curve was then used to evaluate the performance of this calculated Rad-score and determine the optimal truncation value. As shown in **Figure 4**, The AUC values of Rad-score_OS were 0.724 (development cohort) and 0.771 (validation cohort), and the optimal truncation value corresponding to the maximum Jorden index was -8.634; The AUC values of Rad-score_PFS were 0.781 (development cohort) and 0.803 (validation cohort), and the optimal truncation value corresponding to the maximum Jorden index was -13.30.

The developed radiomics signature was significantly related to the poor prognosis of PDAC patients

According to the optimal truncation value, all patients were then divided into high Rad-score group and low Rad-score group. After comparative analysis, we found that, in the development cohort, there were significant differences between the high Rad-score_OS group and the low Rad-score_OS group on tumor location, dif-

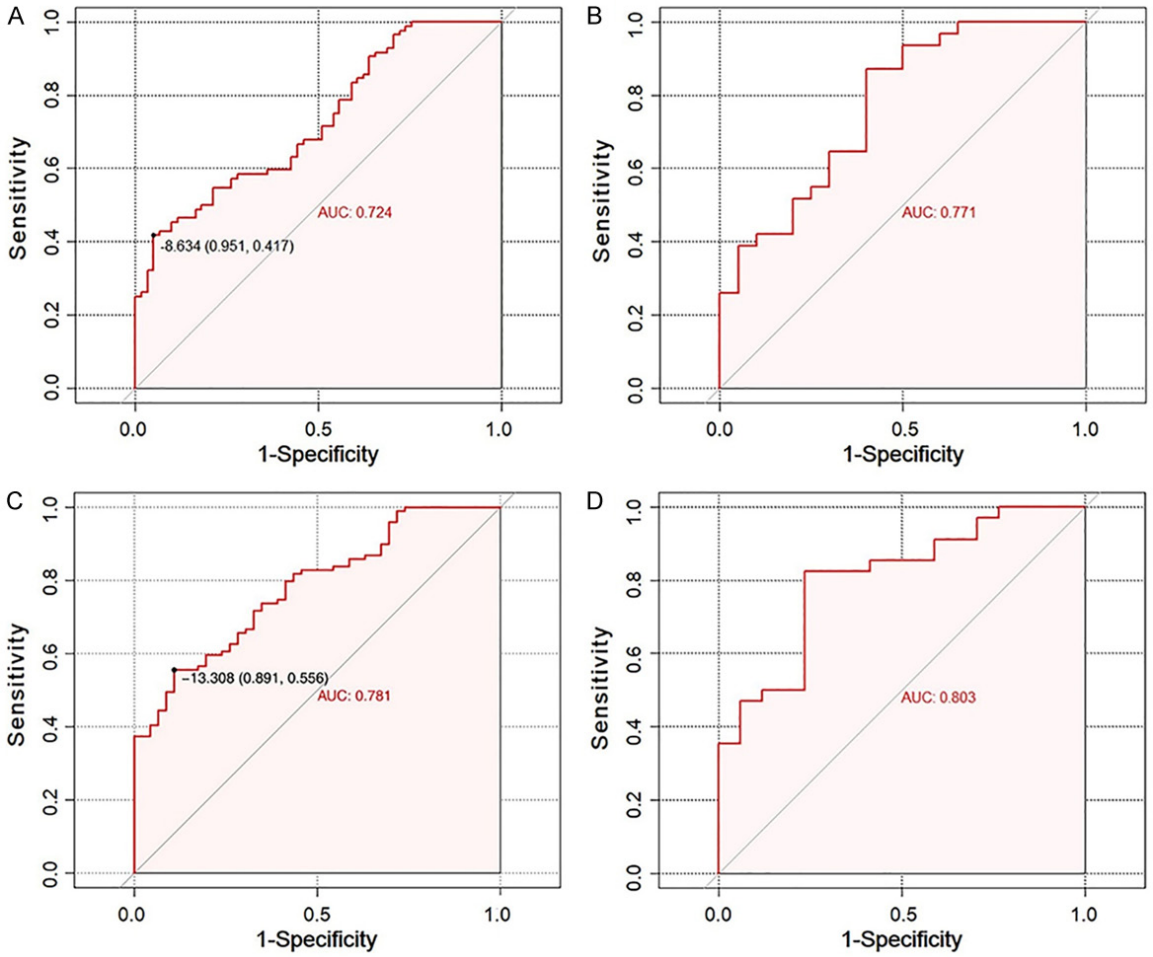

Figure 4. The performance of radiomics signature was evaluated by ROC curve. The ROC curve of OS-related radiomics signature in development cohort and validation cohort is shown in (A) (AUC = 0.724, the optimal truncation value = -8.634) and (B) (AUC = 0.771), respectively. The ROC curve of PFS-related radiomics signature in development cohort and validation cohort is shown in (C) (AUC = 0.781, the optimal truncation value = -13.308) and (D) (AUC = 0.803), respectively.

ferentiated degree, AJCC staging, N staging, vascular invasion and CA19-9 level, and significant differences were also existed between the two groups on tumor location, differentiated degree and nerve invasion in the validation cohort (**Table 3**). In addition, our results also indicated that, both in the development and validation cohorts, there were significant differences on tumor location, differentiated degree and AJCC staging between the high Rad-score_PFS group and the low Rad-score_PFS group, as detailed in **Table 4**. Furthermore, our results also indicated that, compared with high Rad-score_PFS group, the patients in the low Rad-score_PFS group had a significant lower incidence of recurrence and metastasis (**Table 4**).

Subsequently, we further analyzed the influence of radiomics signature on patients' OS and PFS, and the results illustrated that the OS and PFS of PDAC patients in the low Rad-score group were significantly better than those in the high Rad-score group (**Figure 5**), which indicated that the radiomics signature was strongly associated with the poor outcomes of PDAC patients.

The developed clinical-radiomics nomogram outperformed traditional models in evaluating the prognosis of patients with PDAC

After univariate Cox regression analysis, we found that differentiated degree, AJCC staging, N staging, vascular invasion, level of CEA and CA19-9, therapeutic regimen and Rad-score were significant risk factors affecting OS and PFS (**Table 5**). The above significant risk factors were then brought into the multivariate Cox

Table 3. Correlation analysis of OS-related radiomics signature with clinical parameters

Variables	Development cohort (*n* = 145)			Validation cohort (*n* = 51)		
	Low Rad-score group	High Rad-score group	*P*	Low Rad-score group	High Rad-score group	*P*
Gender			0.491			0.693
Male	55	22		21	8	
Female	52	16		17	5	
Age, years			0.257			0.286
≤ 60	42	11		15	3	
> 60	65	27		23	10	
Tumor location			0.009			0.005
head	97	28		34	7	
body and tail	10	10		4	6	
Maximum diameter of tumor			0.965			0.811
≤ 4 cm	68	24		19	6	
> 4 cm	39	14		19	7	
Differentiated degree			< 0.001			0.014
High	15	0		7	0	
Medium	75	17		25	6	
Low	17	21		6	7	
AJCC staging			< 0.001			0.085
I	23	0		7	0	
II	73	23		27	9	
III	11	15		4	4	
T staging			0.643			0.869
T1	16	8		5	1	
T2	52	16		14	5	
T3	39	14		19	7	
N staging			< 0.001			0.120
N0	42	7		15	2	
N1	53	16		19	7	
N2	12	15		42	4	
Vascular invasion			0.007			0.121
No	61	12		24	5	
Yes	46	26		14	8	
Nerve invasion			0.325			0.017
No	55	16		26	4	
Yes	52	22		12	9	
BMI (Kg/m^2)			0.743			0.940
< 24	54	18		20	7	
≥ 24	53	20		18	6	
CEA (ng/ml)			0.053			0.159
≤ 5	31	5		10	1	
> 5	76	33		28	12	
CA19-9 (U/ml)			0.010			0.577
≤ 37	54	10		18	5	
> 37	53	28		20	8	
Smoking history			0.715			0.363
No	82	28		24	10	
Yes	25	10		14	3	

Drinking history			0.655			0.650
No	80	27		26	8	
Yes	27	11		12	5	
Hypertension			0.595			0.756
No	71	27		28	9	
Yes	36	11		10	4	
Diabetes			0.777			0.756
No	85	31		28	9	
Yes	22	7		10	4	
Clinical symptoms			0.936			0.433
No	6	2		3	2	
Yes	101	36		35	11	

Table 4. Correlation analysis of PFS-related radiomics signature with clinical parameters

Variables	Development cohort (*n* = 145)			Validation cohort (*n* = 51)		
	Low Rad-score group	High Rad-score group	*P*	Low Rad-score group	High Rad-score group	*P*
Gender			0.963			0.424
Male	45	32		18	11	
Female	40	28		16	6	
Age, years			0.283			1.000
≤ 60	28	25		12	6	
> 60	57	35		22	11	
Tumor location			0.021			0.046
head	78	47		30	11	
body and tail	7	13		4	6	
Maximum diameter of tumor			0.469			0.428
≤ 4 cm	56	36		18	7	
> 4 cm	29	24		16	10	
Differentiated degree			< 0.001			0.015
High	15	0		7	0	
Medium	59	33		22	9	
Low	11	27		5	8	
AJCC staging			< 0.001			0.038
I	21	2		7	0	
II	57	39		24	12	
III	7	19		3	5	
T staging			0.737			0.582
T1	14	10		5	1	
T2	42	26		13	6	
T3	29	24		16	10	
N staging			0.002			0.084
N0	35	14		14	3	
N1	42	27		17	9	
N2	8	19		3	5	
Vascular invasion			0.006			0.318
No	51	22		21	8	
Yes	34	38		13	9	

Nerve invasion			0.070			0.003
No	47	24		25	5	
Yes	38	36		9	12	
BMI (Kg/m^2)			0.106			1.000
< 24	47	25		18	9	
≥ 24	38	35		16	8	
CEA (ng/ml)			0.459			0.229
≤ 5	23	13		9	2	
> 5	62	47		25	15	
CA19-9 (U/ml)			0.011			0.320
≤ 37	45	19		17	6	
> 37	40	41		17	11	
Smoking history			0.849			0.294
No	64	46		21	13	
Yes	21	14		13	4	
Drinking history			0.916			0.834
No	63	44		23	11	
Yes	22	16		11	6	
Hypertension			0.358			0.824
No	60	38		25	12	
Yes	25	22		9	5	
Diabetes			1.000			0.375
No	68	48		26	11	
Yes	17	12		8	6	
Clinical symptoms			0.333			0.739
No	6	2		3	2	
Yes	79	58		31	15	
Recurrence and/or metastasis			< 0.001			0.019
No	69	31		27	8	
Yes	16	29		7	9	

regression model, and the results showed that the levels of CEA and CA19-9, therapeutic regimen and Rad-score_OS (HR: 4.495, 95% CI: 2.315~8.729, P < 0.001) were independent prognostic factors affecting OS, while the differentiated degree, CA19-9 level and Rad-score_PFS (HR: 3.821, 95% CI: 1.859~7.852, P < 0.001) were independent prognostic factors affecting PFS (**Table 6**). Based on the above independent prognostic risk factors, two clinical-radiomics nomograms were developed to predict OS and PFS, respectively (**Figure 6**).

Subsequently, three methods were used to evaluate the performance of the developed clinical-radiomics nomograms. First, the calibration curves shown in **Figure 7A-D** indicated adequate consistency between estimated risks using the nomograms and the actual observed outcomes in the two cohorts. Then, we developed another two models, a traditional AJCC staging system model and a clinical model containing only clinical characteristics which were independently related to worse OS and PFS, the results showed that, both in the development and validation cohorts, the C-index values of the clinical-radiomics nomograms (OS: $C\text{-index}_{\text{Development cohort}} = 0.814$, $C\text{-index}_{\text{Validation cohort}} = 0.790$; PFS: $C\text{-index}_{\text{Development cohort}} = 0.767$, $C\text{-index}_{\text{Validation cohort}} = 0.757$) were higher than the two traditional models (**Table 7**), suggesting that our developed clinical-radiomics nomograms outperformed clinical model and AJCC staging system model in terms of survival estimation in PDAC patients. Finally, the results of DCA suggested that the clinical-radiomics nomograms generated more clinical net benefit at most threshold probabilities (**Figure 7E** and **7F**), which further verified the efficient predictive power of the nomograms.

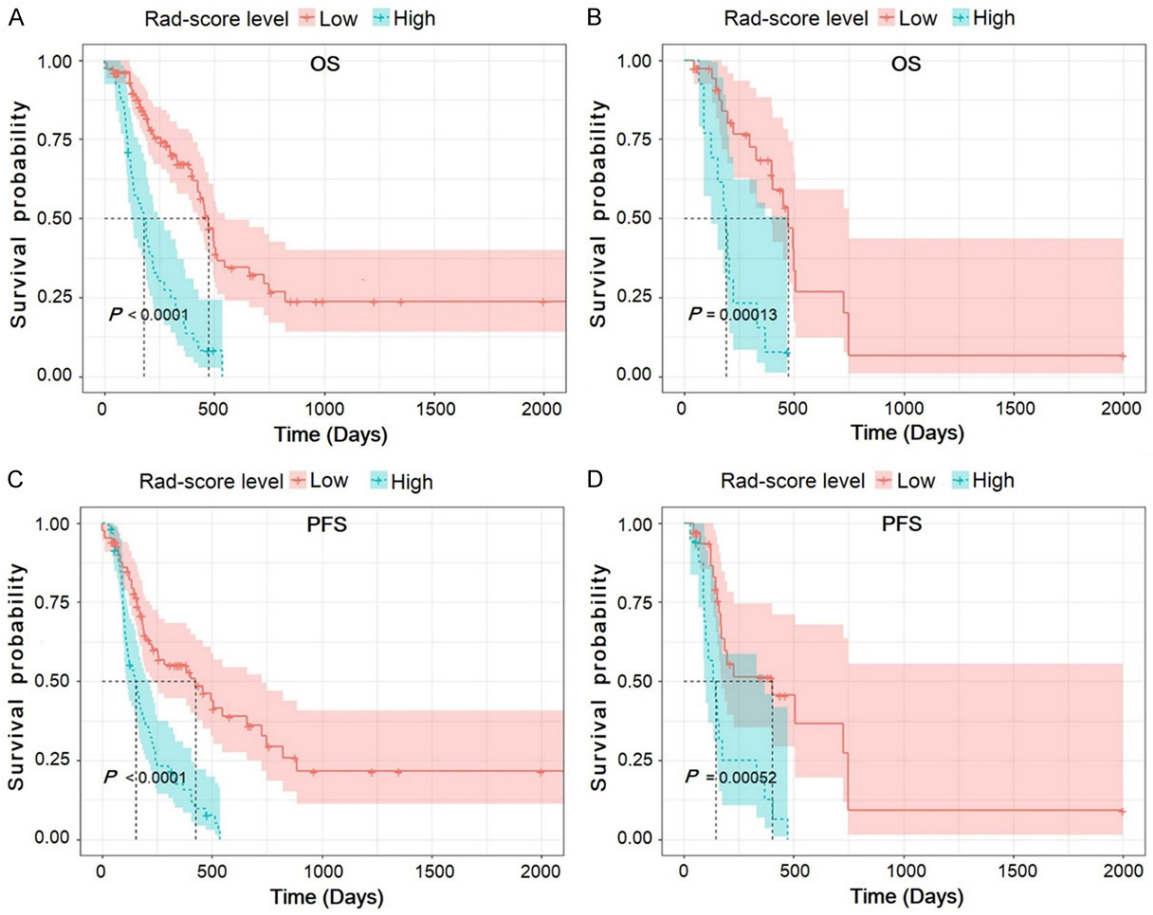

Figure 5. Kaplan-Meier analysis according to the optimal truncation value of Rad-score in development cohort (left pane) and validation cohort (right pane). A, B. OS; C, D. PFS.

Discussion

PDAC is a highly heterogeneous malignant tumor, and the prognosis of PDAC patients in identical stages vary greatly [20, 21]. Neoadjuvant therapy may be an ideal choice for PDAC patients with poor prognosis, and the National Comprehensive Cancer Network guideline recommends neoadjuvant chemotherapy for high risk resectable PDAC patients [22]. Therefore, accurate prognostic assessment is crucially important for the identification of those patients who might benefit from preoperative treatments, and it could help clinicians to make individualized and efficient antineoplastic regimens. However, we have to face a practical problem that there is no ideal preoperative biomarker or model to predict the prognosis of PDAC patients except CA19-9, a severely limited biomarker [23].

Currently, radiomics has been widely explored in survival estimation of different types of cancers including non-small cell lung cancer, breast cancer, gastric cancer and PDAC [16, 24-27], but almost all of the previously developed radiomics nomograms for survival prediction of PDAC patients were based on CT [16, 28-32]. In the study of Xie T. *et al.*, Rad-score was identified as an independent prognostic factor in PDAC patients, and the CT-based radiomics nomogram which integrated Rad-score and clinical data provided better prognostic prediction in patients with resected PDAC [16]. Cen C. *et al.* constructed a nomogram model that combined clinical characteristics and radiomics signatures which were extracted from arterial phase or portal venous phase images of contrast-enhanced CT, they demonstrated that the nomogram model had an excellent performance in predicting OS of PDAC patients [31]. However, studies on developing a radiomics nomogram based on MRI to predict the prognosis of preoperative PDAC patients was rare.

Table 5. Univariate Cox regression analysis of risk factors associated with OS and PFS from the development cohort

Variables	OS			PFS		
	HR	95% CI	*P*	HR	95% CI	*P*
Gender			0.491			0.571
Male	1			1		
Female	1.163	0.756~1.79		1.121	0.754~1.667	
Age, years			0.333			0.457
≤ 60	1			1		
> 60	1.25	0.796~1.962		0.858	0.574~1.284	
Tumor location			0.998			0.698
head	1			1		
body and tail	1.001	0.517~1.94		1.119	0.633~1.978	
Maximum diameter of tumor			0.515			0.853
≤ 4 cm	1			1		
> 4 cm	0.859	0.543~1.358		1.04	0.684~1.582	
Differentiated degree			< 0.001			< 0.001
High	1			1		
Medium	1.938	0.874~4.299		2.037	0.958~4.329	
Low	15.773	6.321~39.355		22.944	9.238~56.988	
AJCC staging			< 0.001			< 0.001
I	1			1		
II	3.796	1.848~7.799		3.677	1.888~7.163	
III	14.125	5.893~33.856		14.420	6.503~31.976	
T staging			0.663			0.839
T1	1			1		
T2	0.84	0.484~1.46		0.859	0.507~1.454	
T3	0.762	0.423~1.373		0.933	0.535~1.629	
N staging			< 0.001			< 0.001
N0	1			1		
N1	3.61	2.038~6.394		3.215	1.905~5.426	
N2	7.641	3.874~15.072		7.443	4.030~13.744	
Vascular invasion			0.030			0.044
No	1			1		
Yes	1.618	1.049~2.497		1.506	1.011~2.245	
Nerve invasion			0.103			0.021
No	1			1		
Yes	1.432	0.93~2.204		1.598	1.073~2.381	
BMI (Kg/m^2)			0.889			0.720
< 24	1			1		
≥ 24	1.031	0.671~1.585		1.076	0.722~1.603	
CEA (ng/ml)			0.001			0.010
≤ 5	1			1		
> 5	2.468	1.458~4.175		1.851	1.160~2.953	
CA19-9 (U/ml)			< 0.001			< 0.001
≤ 37	1			1		
> 37	2.971	1.885~4.683		3.390	2.201~5.221	
Smoking history			0.406			0.860
No	1			1		
Yes	0.776	0.426~1.413		1.047	0.630~1.740	

Drinking history			0.824			0.933
No	1			1		
Yes	0.944	0.566~1.573		1.020	0.644~1.616	
Hypertension			0.208			0.722
No	1			1		
Yes	0.734	0.454~1.188		0.925	0.603~1.419	
Diabetes			0.859			0.403
No	1			1		
Yes	1.05	0.616~1.788		1.234	0.754~2.017	
Clinical symptoms			0.283			0.142
No	1			1		
Yes	1.737	0.633~4.766		2.128	0.776~5.830	
Therapeutic regimen			< 0.001			0.022
Surgery alone	1			1		
Surgery + chemotherapy	0.345	0.217~0.547		0.554	0.362~0.847	
Surgery + radiotherapy	0.481	0.147~1.578		0.650	0.199~2.125	
Surgery + chemoradiotherapy	0	0~3.345		0.945	0.228~3.922	
Other	0.188	0.066~0.534		0.288	0.113~0.734	
Rad-score	10.386	5.785~18.648	< 0.001	11.213	6.007~20.932	< 0.001

In this study, we retrospectively enrolled 196 PDAC patients from two independent centers, based on the clinical data of these cases, we identified several optimal radiomics features, especially "wavelet.HLH_glcm_Imc2" and "wavelet.LHH_glcm_Imc2" which robustly reflected the OS and PFS of PDAC patients, and most of these radiomics features included high-order radiomic features, such as GLCM, which measured the spatial relationship between local nearby pixels and potentially reflected the biological characteristics and heterogeneity of tumors [17, 33]. Moreover, in addition to CA19-9 and the degree of differentiation, previous study had demonstrated that the AJCC staging system was suitable for resected PDAC patients, and the N staging had superior accuracy in predicting survival than T staging [34], which was further verified in this study. However, the use of a single clinical characteristic to predict the prognosis of PDAC patients was insufficient, because it was likely to oversimplify the complexity of biological behaviors of tumors. Therefore, it is necessary to construct a multiomics model to efficiently and accurately evaluate the prognosis of PDAC patients. Based on this, we then developed a novel preoperative clinical-radiomics nomogram which incorporated clinical parameters and radiomics signatures extracted from MRI images, our results indicated that the developed MRI-based radiomics nomogram displayed a greater net benefit than traditional prognostic prediction models, and it might act as an individual and easy-to-use model for prognosis prediction in patients with PDAC.

However, this study has several limitations. First, although we performed standardized preprocessing of MRI images for each patient, it was inevitable that there was still some heterogeneity due to the retrospective nature of the study. Second, only T2WI sequence was used and analyzed in this study, if multiple sequence images of MRI can be used to develop the nomogram without additional bias, it is possible to more truly reflect the characteristics of PDAC. Third, the median follow-up was 222 days in this study with relatively small sample size, future prospective trials with a longer follow-up and a larger sample size are needed to validate and optimize our clinical-radiomics nomogram so as to provide more accurate prognostic predictions.

Conclusions

In this retrospective prognostic study, we developed and externally validated a preoperative clinical-radiomics nomogram which incorporated the radiomics signature and several clinical parameters for PDAC survival prediction. The results suggested that the developed clinical-radiomics nomogram outperformed traditional models in evaluating the prognosis of patients with PDAC, and it might assist clinicians in determining personalized therapeutic regimen

Table 6. Multivariate Cox regression analysis of independent risk factors associated with OS and PFS from the development cohort

Variables	OS			PFS		
	HR	95% CI	*P*	HR	95% CI	*P*
Differentiated degree			0.053			0.003
High	1			1		
Medium	0.864	0.331~2.256		1.077	0.404~2.868	
Low	3.708	1.018~13.508		5.289	1.475~18.965	
N staging			0.290			0.416
N0	1			1		
N1	1.997	0.984~4.053		1.602	0.833~3.081	
N2	0.911	0.068~12.182		0.208	0.014~3.192	
Vascular invasion			0.815			0.757
No	1			1		
Yes	1.026	0.644~1.635		0.828	0.517~1.324	
Nerve invasion			–			0.861
No		–		1		
Yes				0.920	0.569~1.489	
CEA (ng/ml)			0.017			0.276
≤ 5	1			1		
> 5	1.702	0.791~3.662		1.130	0.564~2.262	
CA19-9 (U/ml)			0.011			0.022
≤ 37	1			1		
> 37	1.940	0.939~4.009		1.825	0.958~3.478	
Therapeutic regimen			0.002			0.175
Surgery alone	1			1		
Surgery + chemotherapy	0.326	0.198~0.536		0.780	0.502~1.211	
Surgery + radiotherapy	0.261	0.056~1.208		1.822	0.312~10.649	
Surgery + chemoradiotherapy	0	0~1.299		2.072	0.453~9.477	
Other	0.242	0.081~0.717		0.504	0.186~1.364	
Rad-score	4.495	2.315~8.729	< 0.001	3.821	1.859~7.852	< 0.001

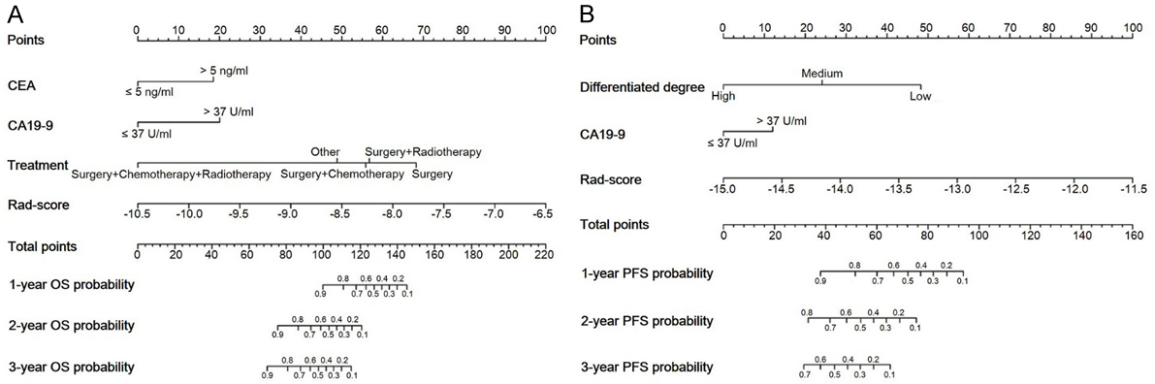

Figure 6. The developed clinical-radiomics nomogram incorporating the Rad-score and clinical parameters to predict OS (A) and PFS (B) for PDAC patients. The OS-related radiomics signature or PFS-related radiomics signature of PDAC patient is located on the Rad-score axis, the point for each variable was achieved by drawing a line straight upward to the point axis, and the points of variables were then summed. The final sum is located on the total points axis, then a line is drawn down to find out the 1/2/3-year OS or PFS probability.

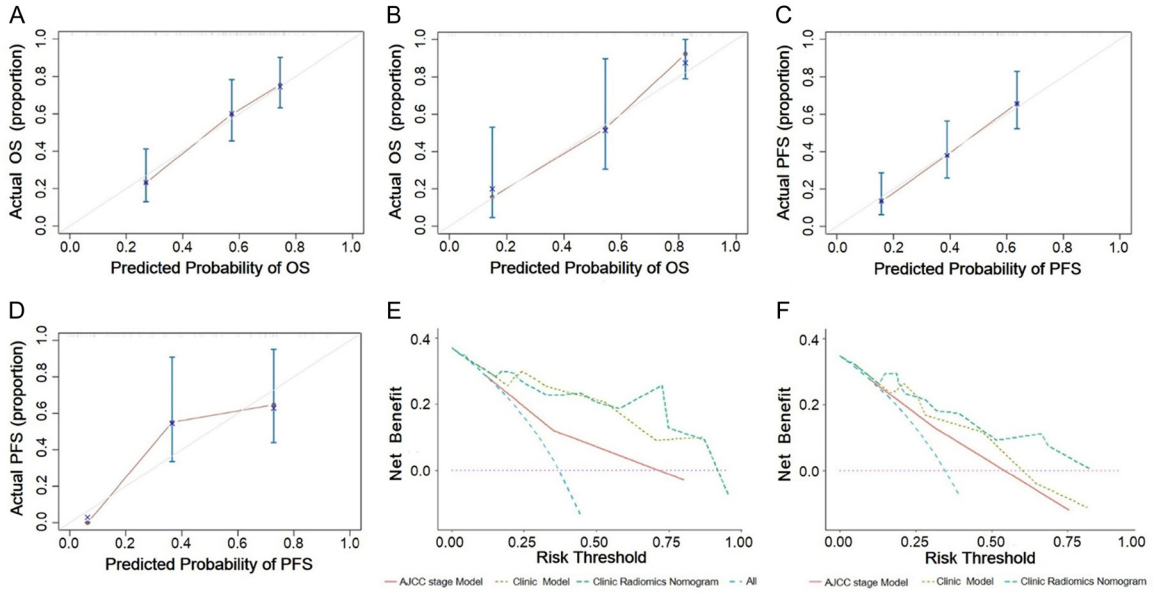

Figure 7. Calibration curves and decision-curve analysis of the clinical-radiomics nomogram. The consistency of predicted OS with actual OS in the development and validation cohorts are shown in (A and B), respectively. The consistency of predicted PFS with actual PFS in the development and validation cohorts are shown in (C and D), respectively. OS or PFS predicted by the clinical-radiomics nomogram is plotted on the x-axis, and the actual OS or PFS is plotted on the y-axis, the gray diagonal line represents the reference line showing the "ideal" prediction, the red line represents the performance of the clinical-radiomics nomogram in prognostic prediction, the closer the red line is to the gray diagonal line, the higher the consistency between the predicted results and the actual results. (E and F) Represent the decision-curve analysis for OS and PFS, respectively. The threshold probability is shown on the x-axis and the net benefit is shown on the y-axis, the clinical-radiomics nomogram (green dotted line) achieves the highest net benefit compared to AJCC staging system model (red line), clinical model (yellow dotted line), treat-all strategy (blue dotted line), and the treat-none strategy (horizontal red dotted line).

Table 7. The C-index values of the developed clinical-radiomics nomogram and other two traditional models

	Models	Development cohort (n = 145)		Validation cohort (n = 51)	
		C-index	95% CI	C-index	95% CI
OS	Clinical-Radiomics nomogram	0.814	0.769~0.859	0.790	0.714~0.866
	Traditional AJCC staging model	0.689	0.636~0.742	0.655	0.563~0.747
	Traditional clinical model	0.798	0.757~0.839	0.758	0.685~0.831
PFS	Clinical-Radiomics nomogram	0.767	0.724~0.810	0.757	0.677~0.837
	Traditional AJCC staging model	0.690	0.641~0.739	0.654	0.554~0.754
	Traditional clinical model	0.741	0.700~0.782	0.707	0.631~0.783

selections for PDAC patients. However, the clinical-radiomics nomogram still require further calibration and validation using a large and high-quality prospective study.

Acknowledgements

This work was supported by the National Natural Science Foundation of China under Grant 81972845; Introduction of Specialist Team in Clinical Medicine of Xuzhou under Grant 2019TD003; Xuzhou Key Research and Development Program undere Grant KC21168.

Disclosure of conflict of interest

None.

Address correspondence to: Longzhen Zhang and Xin Ding, Department of Radiation Oncology, Affiliated Hospital of Xuzhou Medical University, No. 9 Kunpeng North Road, Xuzhou 221000, Jiangsu, China. Tel: +86-15895236960; E-mail: jsxyfyzlz@

126.com (LZZ); Tel: +86-13952206201; E-mail: dingxin81@163.com (XD)

References

[1] Ducreux M, Cuhna AS, Caramella C, Hollebecque A, Burtin P, Goere D, Seufferlein T, Haustermans K, Van Laethem JL, Conroy T and Arnold D; ESMO Guidelines Committee. Cancer of the pancreas: ESMO Clinical Practice Guidelines for diagnosis, treatment and follow-up. Ann Oncol 2015; 26 Suppl 5: v56-68.

[2] Puleo F, Nicolle R, Blum Y, Cros J, Marisa L, Demetter P, Quertinmont E, Svrcek M, Elarouci N, Iovanna J, Franchimont D, Verset L, Galdon MG, Deviere J, de Reynies A, Laurent-Puig P, Van Laethem JL, Bachet JB and Marechal R. Stratification of pancreatic ductal adenocarcinomas based on tumor and microenvironment features. Gastroenterology 2018; 155: 1999-2013.

[3] Yu KH, Ozer M, Cockrum P, Surinach A, Wang S and Chu BC. Real-world prognostic factors for survival among treated patients with metastatic pancreatic ductal adenocarcinoma. Cancer Med 2021; 10: 8934-8943.

[4] Huang L, Jansen L, Balavarca Y, Molina-Montes E, Babaei M, van der Geest L, Lemmens V, Van Eycken L, De Schutter H, Johannesen TB, Fristrup CW, Mortensen MB, Primic-Zakelj M, Zadnik V, Becker N, Hackert T, Magi M, Cassetti T, Sassatelli R, Grutzmann R, Merkel S, Goncalves AF, Bento MJ, Hegyi P, Lakatos G, Szentesi A, Moreau M, van de Velde T, Broeks A, Sant M, Minicozzi P, Mazzaferro V, Real FX, Carrato A, Molero X, Besselink MG, Malats N, Buchler MW, Schrotz-King P and Brenner H. Resection of pancreatic cancer in Europe and USA: an international large-scale study highlighting large variations. Gut 2019; 68: 130-139.

[5] Kim JR, Kim H, Kwon W, Jang JY and Kim SW. Pattern of local recurrence after curative resection in pancreatic ductal adenocarcinoma according to the initial location of the tumor. J Hepatobiliary Pancreat Sci 2021; 28: 105-114.

[6] Healy GM, Salinas-Miranda E, Jain R, Dong X, Deniffel D, Borgida A, Hosni A, Ryan DT, Njeze N, McGuire A, Conlon KC, Dodd JD, Ryan ER, Grant RC, Gallinger S and Haider MA. Pre-operative radiomics model for prognostication in resectable pancreatic adenocarcinoma with external validation. Eur Radiol 2022; 32: 2492-2505.

[7] Malleo G, Maggino L, Ferrone CR, Marchegiani G, Luchini C, Mino-Kenudson M, Paiella S, Qadan M, Scarpa A, Lillemoe KD, Bassi C, Fernandez-Del Castillo C and Salvia R. Does site matter? Impact of tumor location on pathologic characteristics, recurrence, and survival of resected pancreatic ductal adenocarcinoma. Ann Surg Oncol 2020; 27: 3898-3912.

[8] Park JK, Paik WH, Ryu JK, Kim YT, Kim YJ, Kim J, Song BJ, Park JM and Yoon YB. Clinical significance and revisiting the meaning of CA 19-9 blood level before and after the treatment of pancreatic ductal adenocarcinoma: analysis of 1,446 patients from the pancreatic cancer cohort in a single institution. PLoS One 2013; 8: e78977.

[9] Cassinotto C, Chong J, Zogopoulos G, Reinhold C, Chiche L, Lafourcade JP, Cuggia A, Terrebonne E, Dohan A and Gallix B. Resectable pancreatic adenocarcinoma: role of CT quantitative imaging biomarkers for predicting pathology and patient outcomes. Eur J Radiol 2017; 90: 152-158.

[10] Lambin P, Rios-Velazquez E, Leijenaar R, Carvalho S, van Stiphout RG, Granton P, Zegers CM, Gillies R, Boellard R, Dekker A and Aerts HJ. Radiomics: extracting more information from medical images using advanced feature analysis. Eur J Cancer 2012; 48: 441-446.

[11] Lambin P, Leijenaar RTH, Deist TM, Peerlings J, de Jong EEC, van Timmeren J, Sanduleanu S, Larue R, Even AJG, Jochems A, van Wijk Y, Woodruff H, van Soest J, Lustberg T, Roelofs E, van Elmpt W, Dekker A, Mottaghy FM, Wildberger JE and Walsh S. Radiomics: the bridge between medical imaging and personalized medicine. Nat Rev Clin Oncol 2017; 14: 749-762.

[12] Huang YQ, Liang CH, He L, Tian J, Liang CS, Chen X, Ma ZL and Liu ZY. Development and validation of a radiomics nomogram for preoperative prediction of lymph node metastasis in colorectal cancer. J Clin Oncol 2016; 34: 2157-2164.

[13] Tagliafico AS, Piana M, Schenone D, Lai R, Massone AM and Houssami N. Overview of radiomics in breast cancer diagnosis and prognostication. Breast 2020; 49: 74-80.

[14] Zheng X, Yao Z, Huang Y, Yu Y, Wang Y, Liu Y, Mao R, Li F, Xiao Y, Wang Y, Hu Y, Yu J and Zhou J. Deep learning radiomics can predict axillary lymph node status in early-stage breast cancer. Nat Commun 2020; 11: 1236.

[15] Shi L, He Y, Yuan Z, Benedict S, Valicenti R, Qiu J and Rong Y. Radiomics for response and outcome assessment for non-small cell lung cancer. Technol Cancer Res Treat 2018; 17: 1533033818782788.

[16] Xie T, Wang X, Li M, Tong T, Yu X and Zhou Z. Pancreatic ductal adenocarcinoma: a radiomics nomogram outperforms clinical model and TNM staging for survival estimation after curative resection. Eur Radiol 2020; 30: 2513-2524.

[17] Tang TY, Li X, Zhang Q, Guo CX, Zhang XZ, Lao MY, Shen YN, Xiao WB, Ying SH, Sun K, Yu RS, Gao SL, Que RS, Chen W, Huang DB, Pang PP, Bai XL and Liang TB. Development of a novel

multiparametric mri radiomic nomogram for preoperative evaluation of early recurrence in resectable pancreatic cancer. J Magn Reson Imaging 2020; 52: 231-245.
[18] Liang L, Ding Y, Yu Y, Liu K, Rao S, Ge Y and Zeng M. Whole-tumour evaluation with MRI and radiomics features to predict the efficacy of S-1 for adjuvant chemotherapy in postoperative pancreatic cancer patients: a pilot study. BMC Med Imaging 2021; 21: 75.
[19] Bian Y, Liu YF, Jiang H, Meng Y, Liu F, Cao K, Zhang H, Fang X, Li J, Yu J, Feng X, Li Q, Wang L, Lu J and Shao C. Machine learning for MRI radiomics: a study predicting tumor-infiltrating lymphocytes in patients with pancreatic ductal adenocarcinoma. Abdom Radiol (NY) 2021; 46: 4800-4816.
[20] Stark AP, Sacks GD, Rochefort MM, Donahue TR, Reber HA, Tomlinson JS, Dawson DW, Eibl G and Hines OJ. Long-term survival in patients with pancreatic ductal adenocarcinoma. Surgery 2016; 159: 1520-1527.
[21] Hlavsa J, Cecka F, Zaruba P, Zajak J, Gurlich R, Strnad R, Pavlik T, Kala Z and Lovecek M. Tumor grade as significant prognostic factor in pancreatic cancer: validation of a novel TNMG staging system. Neoplasma 2018; 65: 637-643.
[22] Tempero MA, Malafa MP, Chiorean EG, Czito B, Scaife C, Narang AK, Fountzilas C, Wolpin BM, Al-Hawary M, Asbun H, Behrman SW, Benson AB, Binder E, Cardin DB, Cha C, Chung V, Dillhoff M, Dotan E, Ferrone CR, Fisher G, Hardacre J, Hawkins WG, Ko AH, LoConte N, Lowy AM, Moravek C, Nakakura EK, O'Reilly EM, Obando J, Reddy S, Thayer S, Wolff RA, Burns JL and Zuccarino-Catania G. Pancreatic adenocarcinoma, version 1.2019. J Natl Compr Canc Netw 2019; 17: 202-210.
[23] Goh SK, Gold G, Christophi C and Muralidharan V. Serum carbohydrate antigen 19-9 in pancreatic adenocarcinoma: a mini review for surgeons. ANZ J Surg 2017; 87: 987-992.
[24] Kirienko M, Cozzi L, Antunovic L, Lozza L, Fogliata A, Voulaz E, Rossi A, Chiti A and Sollini M. Prediction of disease-free survival by the PET/CT radiomic signature in non-small cell lung cancer patients undergoing surgery. Eur J Nucl Med Mol Imaging 2018; 45: 207-217.
[25] Park H, Lim Y, Ko ES, Cho HH, Lee JE, Han BK, Ko EY, Choi JS and Park KW. Radiomics signature on magnetic resonance imaging: association with disease-free survival in patients with invasive breast cancer. Clin Cancer Res 2018; 24: 4705-4714.
[26] Jiang Y, Chen C, Xie J, Wang W, Zha X, Lv W, Chen H, Hu Y, Li T, Yu J, Zhou Z, Xu Y and Li G. Radiomics signature of computed tomography imaging for prediction of survival and chemotherapeutic benefits in gastric cancer. EBioMedicine 2018; 36: 171-182.
[27] Yu Y, Tan Y, Xie C, Hu Q, Ouyang J, Chen Y, Gu Y, Li A, Lu N, He Z, Yang Y, Chen K, Ma J, Li C, Ma M, Li X, Zhang R, Zhong H, Ou Q, Zhang Y, He Y, Li G, Wu Z, Su F, Song E and Yao H. Development and validation of a preoperative magnetic resonance imaging radiomics-based signature to predict axillary lymph node metastasis and disease-free survival in patients with early-stage breast cancer. JAMA Netw Open 2020; 3: e2028086.
[28] Park S, Sham JG, Kawamoto S, Blair AB, Rozich N, Fouladi DF, Shayesteh S, Hruban RH, He J, Wolfgang CL, Yuille AL, Fishman EK and Chu LC. CT radiomics-based preoperative survival prediction in patients with pancreatic ductal adenocarcinoma. AJR Am J Roentgenol 2021; 217: 1104-1112.
[29] Zhang Y, Lobo-Mueller EM, Karanicolas P, Gallinger S, Haider MA and Khalvati F. Improving prognostic performance in resectable pancreatic ductal adenocarcinoma using radiomics and deep learning features fusion in CT images. Sci Rep 2021; 11: 1378.
[30] Shi H, Wei Y, Cheng S, Lu Z, Zhang K, Jiang K and Xu Q. Survival prediction after upfront surgery in patients with pancreatic ductal adenocarcinoma: radiomic, clinic-pathologic and body composition analysis. Pancreatology 2021; 21: 731-737.
[31] Cen C, Liu L, Li X, Wu A, Liu H, Wang X, Wu H, Wang C, Han P and Wang S. Pancreatic ductal adenocarcinoma at CT: a combined nomogram model to preoperatively predict cancer stage and survival outcome. Front Oncol 2021; 11: 594510.
[32] Khalvati F, Zhang Y, Baig S, Lobo-Mueller EM, Karanicolas P, Gallinger S and Haider MA. Prognostic value of CT radiomic features in resectable pancreatic ductal adenocarcinoma. Sci Rep 2019; 9: 5449.
[33] Fathi Kazerooni A, Nabil M, Haghighat Khah H, Alviri M, Heidari-Sooreshjaani M, Gity M, Malek M and Saligheh Rad H. ADC-derived spatial features can accurately classify adnexal lesions. J Magn Reson Imaging 2018; 47: 1061-1071.
[34] Hu H, Qu C, Tang B, Liu W, Ma Y, Chen Y, Xie X, Zhuang Y, Gao H, Tian X and Yang Y. Validation and modification of the AJCC 8th TNM staging system for pancreatic ductal adenocarcinoma in a Chinese cohort: a nationwide pancreas data center analysis. Chin J Cancer Res 2021; 33: 457-469.

A

Rad-score_OS = - 0.203855455575152 × original_gldm_DependenceVariance
+ 0.72454502394538 × log.sigma.5.0.mm.3D_glcm_Imc2
+ 0.000594508043691243 × wavelet.LLH_firstorder_10Percentile
+ 0.000600990342680983 × wavelet.LLH_firstorder_Mean
+ 0.673884692402828 × wavelet.LHL_glcm_Correlation
- 0.151955758019423 × wavelet.LHL_glcm_DifferenceEntropy
+ 0.425537714201555 × wavelet.LHL_glszm_ZoneVariance
- 0.664303013620779 × wavelet.LHH_glszm_SmallAreaEmphasis
- 1.66671028113997 × wavelet.HLL_glcm_Imc2
- 0.0011209272237512 × wavelet.HLH_glcm_DifferenceVariance
- 6.69253964336737 × wavelet.HLH_glcm_Imc2
+ 0.000129507265118769 × wavelet.HHL_glcm_ClusterShade

B

Rad-score_PFS = - 0.971744337864066 × original_glrlm_LongRunEmphasis
+ 0.000714077093010009 × wavelet.LLH_firstorder_10Percentile
+ 0.00803497360042782 × wavelet.LLH_firstorder_Kurtosis
+ 0.0461519593789209 × wavelet.LHL_glszm_LargeAreaEmphasis
+ 0.455979566294932 × wavelet.LHL_glszm_ZoneVariance
+ 1.91469264917902 × wavelet.LHH_firstorder_Uniformity
- 12.4534037254967 × wavelet.LHH_glcm_Imc2
- 0.0000017002310856 × wavelet.HLH_glcm_Contrast
- 0.00150286932785517 × wavelet.HLH_glcm_DifferenceVariance
+ 0.000118729830464654 × wavelet.HHL_glcm_ClusterShade
- 0.221256029568318×wavelet.HHL_glszm_LargeAreaLowGrayLevelEmphasis

Supplementary Figure 1. The formula for calculating OS-related Rad-score (A) and PFS-related Rad-score (B).